Electrochimica Acta 226 (2017) 40–45

Contents lists available at ScienceDirect

Electrochimica Acta

journal homepage: www.elsevier.com/locate/electacta

Asymptotic behaviors of the Poisson-Nernst-Planck model, generalizations and best adjust of experimental data

E.K. Lenzi [a], R.S. Zola [b,c], R. Rossato [c], H.V. Ribeiro [b], D.S. Vieira [b], L.R. Evangelista [b]

[a] Departamento de Física, Universidade Estadual de Ponta Grossa, Av. Carlos Cavalcanti 4748, 84030-900 Ponta Grossa, Paraná, Brazil
[b] Departamento de Física, Universidade Estadual de Maringá, Avenida Colombo 5790, 87020-900 Maringá, Paraná, Brazil
[c] Departamento de Física, Universidade Tecnológica Federal do Paraná - Apucarana, PR 86812-460, Brazil

ARTICLE INFO

Article history:
Received 23 August 2016
Received in revised form 4 December 2016
Accepted 11 December 2016
Available online 24 December 2016

Keywords:
Electrical response
Impedance models
Boundary conditions

ABSTRACT

We analyze the asymptotic behavior of the impedance (or immittance) spectroscopy response of an electrolytic cell in a finite-length situation obtained from the Poisson-Nernst-Planck (PNP) diffusional model and extensions by taking into account different surface effects. The analysis starts with the case characterized by perfect blocking electrodes and proceeds by considering non-blocking conditions on electrodes surface. We argue that the imaginary part of the impedance may be directly related to the boundary condition on the electrode surface, such as charge accumulation and/or transfer by electrochemical reaction or adsorption-desorption processes. We also compare the theoretical predictions with experimental data obtained for a weak electrolytic solution of $KClO_3$.

© 2016 Published by Elsevier Ltd.

1. Introduction

The continuous research and development of state-of-art materials and their electrochemical properties is a burgeoning area of science. It has contribute to a considerable progress in batteries [1–4], fuel cells [5–9], colloidal systems [10–13], oxygen-separation membranes [14,15], electrochemical sensors, functional polymers and biological tissues [16–19]. In this context, among the characterization methods often used, the impedance spectroscopy technique is quite popular. This is mainly due to the possibility of obtaining results related to complex variables (such as mass transfer and chemical reaction rates) via simple measurements.

Despite the deviations between experimental data and theoretical predictions, results from impedance spectroscopy are usually investigated in the framework of the Poisson–Nernst–Planck (PNP) model and/or equivalent circuits. These disagreements are especially remarkable in the low frequency limit, where the PNP and equivalent circuits with simple elements predict an asymptotic impedance $\mathcal{Z}$ characterized by a power-law dependence in the frequency ω with a unitary exponent (*i.e.*, $\mathcal{Z}\sim 1/(i\omega)$) but the experimental data usually exhibit a different power-law regime. These discrepancies are, therefore, strong motivation for investigating extensions/generalizations of the PNP model as well as of the equivalent circuits. For the PNP model, an important possibility is to consider that the diffusive dynamics of the ions is anomalous, which can be done via fractional derivatives [20]. Another relevant aspect to consider in the PNP model is the inherent complexity of the surface effects, which can be taken into account by generalizing the boundary conditions [21]. Regarding equivalent circuits, a typical extension is to use constant phase elements (CPE), in order to account for surface polarization effects [22–24].

In order to achive a suitable description for impedance spectroscopy data, it is crucial to understand the behavior of these generalized models in insightful situations, a task that has not been accomplished yet. An example is the low frequency limit, which is directly connected to the surface effects. Thus, one can find relationships between these behavior of the models and low frequency-relevant experimental aspects such as charge accumulation, charge transfer by electrochemical reaction, or adsorption–desorption processes. In order fill this gap, we devote this work to investigate the asymptotic behavior of the impedance calculated from extensions of the PNP models in the low frequency limit. We start by considering the case of perfect blocking electrodes, followed by the cases characterized by non-blocking electrodes. The influence of the physical chemistry properties of the model (such as mobility and number of particles) on the electrical response is obtained and compared with experimental data. These analyzes are explored in the Sec. 2 and 3, while the discussions and conclusions are presented in Sec. 4.

2. PNP Impedance Model and Boundary Conditions

We start by reviewing the Poisson-Nernst-Planck (PNP) diffusional model that is usually applied to describe the electrical response. We consider this model subjected to perfect blocking boundary, *i.e.*, $\mathcal{J}_{\pm}\left(\pm d/2, t\right) = 0$, where $\mathcal{J}_{\pm}(z,t)$ is the

http://dx.doi.org/10.1016/j.electacta.2016.12.075
0013-4686/© 2016 Published by Elsevier Ltd.

drift-diffusion current density related to the positive (+) and negative (−) ions, with the electrodes placed at the positions $z = \pm d/2$. The PNP model is characterized by the continuity equation

$$\frac{\partial}{\partial t} n_{\pm}(z,t) = -\frac{\partial}{\partial z} \mathcal{J}_{\pm}(z,t), \tag{1}$$

in connection with

$$\mathcal{J}_{\pm}(z,t) = -\mathcal{D}_{\pm} \frac{\partial}{\partial z} n_{\pm}(z,t) \mp \frac{q\mathcal{D}_{\pm}}{k_B T} n_{\pm}(z,t) \frac{\partial V(z,t)}{\partial z}, \tag{2}$$

where $\mathcal{D}_{+} = \mathcal{D}_{-} = \mathcal{D}$ is the diffusion coefficient (the same for positive and negative ions), $V(z,t)$ is the effective electric potential across a sample of thickness d, k_B is the Boltzmann constant, and T is the absolute temperature. Furthermore, the potential $V(z,t)$ satisfies the Poisson's equation

$$\frac{\partial^2}{\partial z^2} V(z,t) = -\frac{q}{\varepsilon} \left[n_{+}(z,t) - n_{-}(z,t) \right], \tag{3}$$

where ε is the dielectric coefficient of the medium (measured in ε_0 units). At this point it is worth mentioning that other models have also been employed for describing the electrical response of systems. Examples include the Debye-Falkenhagen model [25–27] (that is related to solving a partial differential equation for the potential) and models based on equivalent circuits such as the Randles-Ershler equivalent circuit [28,29].

We can investigate the electrical response of an electrolytic cell by solving these equations. To do so, a periodic potential with a very small amplitude is usually assumed to drive the system. This corresponds to the AC small-signal limit and produce a linear response of the system. Under these assumptions and after some calculations, we obtain the following expression for the impedance

$$\mathcal{Z}_B = \frac{\bar{\mathcal{Z}}}{i\beta^2\psi} \left[\frac{1}{\beta} \tanh\left(\mathcal{M}\beta\right) + i\mathcal{M}\psi \right], \tag{4}$$

with

$$\bar{\mathcal{Z}} = \frac{2\lambda_{\mathcal{D}}}{\omega_{\mathcal{D}}\varepsilon S} \qquad \text{and} \qquad \beta = \sqrt{1 + i\psi}. \tag{5}$$

Here, $\lambda_{\mathcal{D}} = \sqrt{\varepsilon k_B T/(2Nq^2)}$ is the Debye's screening length and S is the electrode area; $\psi = \omega/\omega_{\mathcal{D}}$, $\mathcal{M} = d/(2\lambda_{\mathcal{D}})$, and $\omega_{\mathcal{D}} = \mathcal{D}/\lambda_{\mathcal{D}}^2$ are constants. Notice that Eq. (4) corresponds to a linear response of the system and connects electric quantities with physical-chemical parameters.

We now focus on the asymptotic limit for low frequency of Eq. (4), where the diffusion and surface effects related to the dynamics of the electrolyte particles play an important role. In this limit, where $\psi \to 0$ (*i.e.*, $\omega \to 0$), we have that $1/\beta \sim 1 - i\psi/2$ and can consider $d/\lambda_{\mathcal{D}} \gg 1$, implying that $\tanh(\mathcal{M}\beta) \sim 1$ (see Ref. [30] for more details). Under these assumptions, the main contributions for the real ($R_B = Re(\mathcal{Z})$) and imaginary ($X_B = Im(\mathcal{Z})$) parts of the impedance are

$$R_B \approx \frac{\lambda_{\mathcal{D}}^2 d}{\mathcal{S}\mathcal{D}\varepsilon} \approx \text{const} \tag{6}$$

and

$$X_B \approx -2\frac{\lambda_{\mathcal{D}}}{\omega_{\mathcal{D}}\mathcal{S}\varepsilon\psi}, \tag{7}$$

where the B subscript refers to the perfect blocking boundary condition (see the Appendix A for additional details).

Eqs. (6) and (7) essentially show that R_B and X_B exhibit a resistive and capacitive behavior. The resistive behavior is connected to the bulk effects. On the other hand, the capacitive behavior reflects the boundary conditions assumed on the surface of the electrodes, which only take in account charge accumulation and do not consider other effects such as adsorption–desorption processes and/or charge transfer. These behaviors are illustrated in Fig. 1, where the dependence of Eq. (4) on the frequency is shown.

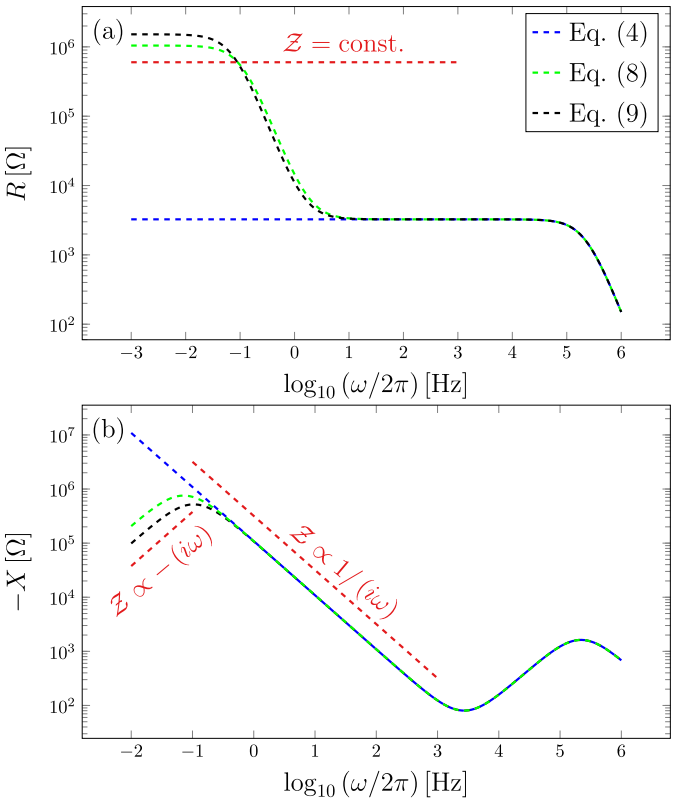

Fig. 1. The behavior of the real ($R = Re(\mathcal{Z})$) and imaginary ($X = Im(\mathcal{Z})$) parts of Eqs. (4), (8), and (9) is illustrated. For simplicity, we have considered $\mathcal{D} = 8 \times 10^{-9}\text{m}^2\text{s}^{-1}$, $\lambda_{\mathcal{D}} = 7.61 \times 10^{-8}$m, $\epsilon = 80\epsilon_0$, $q = 1.6 \times 10^{-19}$C, $S = 3.14 \times 10^{-4}\text{m}^2$, $d = 10^{-3}$m, $\kappa_{\mathcal{J}} = 5 \times 10^{-8}\text{ms}^{-1}$, $\kappa_{\mathcal{O}} = 2 \times 10^{9}(\text{V m s})^{-1}$. We also show red dashed lines as a guide for the asymptotic behavior exhibited by the impedance.

At this point, it is very illustrative to perform a comparison with experimental data to comprehend the range of applicability of Eq. (4). A simple experimental scenario for the electrical response obtained from a weak electrolytic solution of $KClO_3$ ($\approx 2 \times 10^{-3}$ Mol L^{-1}) in Milli– Q deionized water (see Ref. [31,32] for more details on the experimental setup) is shown in Fig. 2 for the electrical impedance. It is evident that the PNP model with perfect blocking boundary conditions is not suitable to describe these experimental data in all range of frequencies. Notice, for instance, that the behavior the experimental data is not purely capacitive ($\mathcal{Z} \propto 1/(i\omega)$) as indicated by the dashed line in Fig. 2, a behavior not predicted by Eq.(4).

The PNP model has also been solved with different boundary conditions on the surfaces such as the Chang–Jaffe [33] ($\mathcal{J}_{\pm}\left(\pm d/2, t\right) = \pm\ \kappa_{\mathcal{J}}\ n_{\pm}\left(\pm d/2, t\right)$) and the Ohmic [34] ($\mathcal{J}_{\pm}\left(\pm d/2, t\right) = \kappa_{\mathcal{O}}\ E\left(\pm d/2, t\right)$). These boundary conditions are related to the conduction current across the electrode, *i.e.*, charge transfer from the electrolyte to the electrode by electrochemical reactions. Under these hypotheses, the impedances for an electrolytic cell are given by

$$\mathcal{Z}_{\mathcal{J}} = \bar{\mathcal{Z}} \frac{\mathcal{M}\psi\beta - i\left[1 + \mathcal{M}\mathcal{H}\left(1 + i\psi\right)\right]\tanh\left(\mathcal{M}\beta\right)}{\beta^2\left\{\psi\beta - i\mathcal{H}\left(1 + i\psi\right)\tanh\left(\mathcal{M}\beta\right)\right\}}, \tag{8}$$

and

$$\mathcal{Z}_{\mathcal{O}} = \frac{1}{\beta^2}\bar{\mathcal{Z}}\mathcal{M}\left[1 - i\frac{1 - \psi_q}{\mathcal{M}\left(\psi - i\psi_q\right)\beta}\tanh\left(\mathcal{M}\beta\right)\right], \tag{9}$$

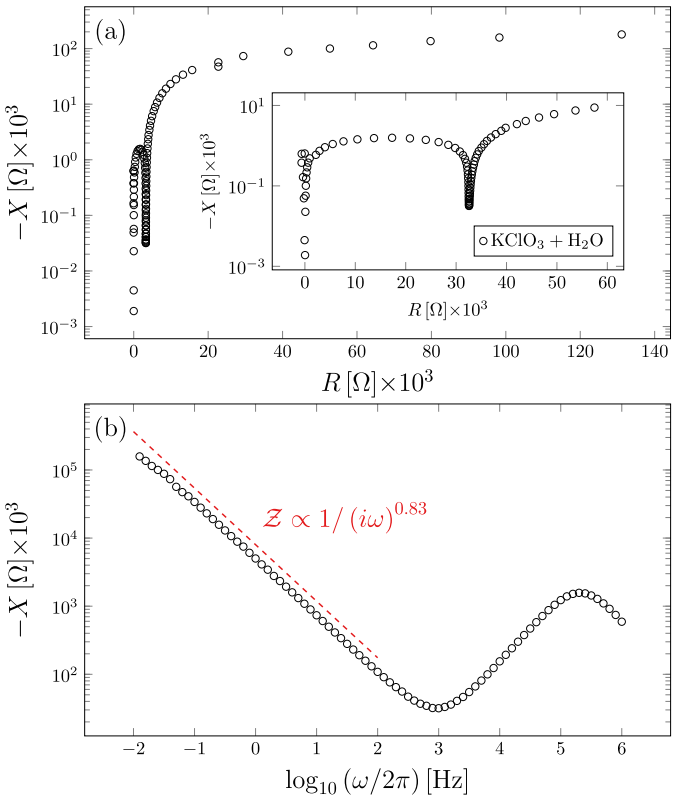

Fig. 2. Behavior of the real ($R = Re(\mathcal{Z})$) and imaginary ($X = Im(\mathcal{Z})$) parts of the impedance of the experimental data obtained from the electrical response of a weak electrolyte of $KClO_3$ (see Ref. [32] for more details on the experimental setup). The relationship between $-X$ and R is illustrated in panel (a), where the inset highlights the behavior for small R. The dependence on the frequency of $-X$ is shown in panel (b), where red dashed line shows the power-law behavior of the data in the low frequency limit. In particular, we observe that the behavior of the experimental data is not purely capacitive ($\mathcal{Z} \propto 1/(i\omega)$, as predicted by the PNP model with perfect blocking boundary conditions), nor purely inductive ($\mathcal{Z} \propto (i\omega)$, as expected for the Chang-Jaffe or Ohmic boundary conditions).

where $\mathcal{H} = \kappa_{CJ}\lambda_{\mathcal{D}}/\mathcal{D}$ and $\psi_q = q\kappa_O/(\epsilon\omega_{\mathcal{D}})$ are constants. Here the subscripts *CJ* and *O* refer to Chang–Jaffe and Ohmic boundary conditions.

After considering the conditions employed in the previous case, we can show that the real and imaginary parts of $\mathcal{Z}_{CJ}$ in the low frequency limit are

$$R_{CJ} \approx \frac{d}{\omega_{\mathcal{D}}\epsilon S} + \frac{\lambda_{\mathcal{D}}}{\kappa_{CJ}}\frac{2\lambda_{\mathcal{D}}}{\epsilon S} = \text{const} \tag{10}$$

and

$$X_{CJ} \approx -\frac{d}{\omega_{\mathcal{D}}\epsilon S}\left(1 + \frac{2\lambda_{\mathcal{D}}^3}{\kappa_{CJ}^2 d}\omega_{\mathcal{D}}^2\left(1 + \frac{2\kappa_{CJ}}{\lambda_{\mathcal{D}}\omega_{\mathcal{D}}}\right)\right)\psi \tag{11}$$

(for details, see Appendix A). Note that the result obtained for R_{CJ} shows that the boundary condition increases the resistance of the electrolytic cell by a constant, *i.e.*, we have an additional term dependent on κ_{CJ}. Furthermore, the frequency behavior exhibited by the imaginary part of the impedance with this boundary condition is completely different. It presents a linear dependence on the frequency, a behavior that is typical of an inductor and contrasts with the capacitive behavior exhibited by the previous case (blocking electrodes). In Fig. 1, the real and imaginary parts of equations (8), and (9) are also plotted and, as to the blocking electrode situation, do not agree with the behavior shown in Fig. 2.

For the Ohmic boundary condition, the real and imaginary parts of the impedance $\mathcal{Z}_O$ in low frequency limit are approximated by

$$R_O \approx \frac{2\lambda_{\mathcal{D}}}{\kappa_O q\mathcal{S}}\left[1 + \frac{\kappa_O q}{\mathcal{D}\varepsilon}\lambda_{\mathcal{D}}^2\left(\frac{d}{2\lambda_{\mathcal{D}}} - 1\right)\right] = \text{const} \tag{12}$$

and

$$X_O \approx -\frac{d}{\omega_{\mathcal{D}}\epsilon S}\left(1 + \frac{\lambda_{\mathcal{D}}\epsilon}{q\kappa_O d}\omega_{\mathcal{D}}\left(1 + \frac{2\epsilon}{q\kappa_O}\omega_{\mathcal{D}}\right)\right)\psi \tag{13}$$

(for details, see Appendix A). These two equations show essentially the behavior of Eqs. (10) and (11) in the low frequency limit (see Fig. 1). This feature suggests that the imaginary part of the impedance, in the low frequency limit, is governed by inductive effects related to the assumption of charge transfer from the electrolyte to the electrode.

The previous results for the PNP model (Eqs. (4), (8), and (9)) show that there are two typical behaviors for the imaginary part of impedance in the low frequency limit: a capacitive (perfect blocking) and an inductive one (Chang-Jaffe and Ohmic). There are several situations that fit these two behaviors. However, there are also experiments that cannot be described by these boundary conditions, as the experimental data show in Fig. 2. This feature suggests that modifications in the bulk equation and/or in boundary conditions are required for archiving a better agreement with experiments.

3. PNP Anomalous Impedance Model

In this section, we consider extensions of the PNP model using fractional time derivatives. The first case to be treated here was extensively discussed in Ref. [35]. It employs fractional time derivatives of distributed order, which are, in general, relevant to describe situations in which two or more diffusive regimes for the mobile charges are present in the bulk system. The main difference between this anomalous case and the usual one is the relaxation process to reach the stationary solution, which is still given in terms of the Boltzmann-Gibbs distribution. The impedance expression obtained with this model is [35]:

$$\mathcal{Z}_F = \frac{\tilde{\mathcal{Z}}}{i\psi\tilde{\beta}^2}\left\{\frac{1}{\tilde{\beta}}\tanh\left(\tilde{\beta}\mathcal{M}\right) + \mathcal{M}\left(\mathcal{A}i\psi + \mathcal{B}\omega_{\mathcal{D}}^{\gamma-1}(i\psi)^{\gamma}\right)\right\}, \tag{14}$$

with

$$\tilde{\beta} = \sqrt{1 + \left(\mathcal{A}i\psi + \mathcal{B}\omega_{\mathcal{D}}^{\gamma-1}(i\psi)^{\gamma}\right)},$$

under the assumptions that $\mathcal{A} \neq 0$ and $\mathcal{B} \neq 0$, with $\mathcal{A} + \mathcal{B} = 1$. The quantities $\mathcal{A}$ and $\mathcal{B}$ are related to the contribution of each fractional differential operator for the diffusion process [35].

In the asymptotic limit of low frequency, the dominant contributions for the real and imaginary parts of Eq. (14) are

$$R_F \approx \frac{d}{\omega_{\mathcal{D}}\mathcal{S}\varepsilon}\left(\mathcal{A} + \frac{\mathcal{B}}{\psi^{1-\gamma}}\omega_{\mathcal{D}}^{\gamma-1}\sin\left(\frac{\pi}{2}\gamma\right)\right) \tag{15}$$

and

$$X_F \approx -2\frac{\lambda_{\mathcal{D}}}{\omega_{\mathcal{D}}\mathcal{S}\varepsilon\psi}\left(1 + \mathcal{M}\psi^{\gamma}\mathcal{B}\omega_{\mathcal{D}}^{\gamma-1}\cos\left(\frac{\pi}{2}\gamma\right)\right). \tag{16}$$

Here the subscript *F* refers to fractional derivatives of this model. It is also worth mentioning that we have employed the approximation $1/\tilde{\beta} \sim 1 - (\mathcal{A}i\psi + \mathcal{B}\,\omega_{\mathcal{D}}^{\gamma-1}\,(i\psi)^{\gamma}\,)/2$ for $\gamma > 1/2$, see the Appendix A for additional details.

The two previous equations show that the changes performed in the bulk (diffusion) equation have a direct impact on the real part of the impedance. For $\gamma \neq 1$, the constant behavior of the real part observed for the three previous cases does not emerge here.

In fact, the behavior is $R_F \propto 1/\psi^{1-\gamma}$ and it is caused by the additional diffusive regime that is not present in the previous cases. On the other hand, the imaginary part of the impedance displays the same behavior of the previous cases, *i.e.*, $X_F \propto 1/\psi$. Thus, the fractional derivatives added to the diffusion equation do not affect the electrical response in the low frequency limit. Theses features are illustrated in Fig. 3.

In order to better understand this model, we can further calculate the high frequency limit, *i.e.*, $\psi \to \infty$. For this case, we consider that $d/\lambda_{\mathcal{D}} >> 1$, $\tanh\left(\mathcal{M}\beta\right) \sim 1$, and the approximations $1/\bar{\beta} \sim \left(1 - 1/F(i\psi)\right) / \left(2\sqrt{F(i\psi)}\right)$ with $1/F(i\psi) \sim \left(1 - \left(\mathcal{B}/\mathcal{A}\right)\omega_{\mathcal{D}}^{\gamma}(i\psi)^{\gamma-1}\right) / \left(\mathcal{A}(i\psi)\right)$. Under these assumptions, the asymptotic behavior is

$$R_F \approx \frac{d}{\omega_{\mathcal{D}}\mathcal{S}\varepsilon\psi^2\mathcal{A}}\left(1 + \frac{\mathcal{B}\omega_{\mathcal{D}}^{\gamma-1}}{\mathcal{A}\psi^{1-\gamma}}\sin\left(\frac{\pi}{2}\gamma\right)\right) \tag{17}$$

and

$$X_F \approx -\frac{d}{\omega_{\mathcal{D}}\mathcal{S}\varepsilon\psi}\left(1 + \frac{\mathcal{B}\omega_{\mathcal{D}}^{\gamma-1}}{\mathcal{A}^2\psi^{2-\gamma}}\cos\left(\frac{\pi}{2}\gamma\right)\right) \quad . \tag{18}$$

From these two expressions, we note that the behavior of the real and imaginary parts of the impedance are essentially the same observed for the standard models. Again, these results suggest that the effect of the fractional operator (combined with the usual one), plays an important role in the low frequency limit for the real part of the impedance. It is also worth remarking that the fractional derivative model of Eq. (14) (as well as the cases of perfect blocking, Chang–Jaffe, and the Ohmic boundary conditions) cannot reproduce the experimental behavior reported in Fig. 2, *i.e.*, the imaginary part of the impedance of these data is not purely capacitive.

These discrepancies with experimental data indicate that the surface effects play an important role in the modeling, especially in the low frequency limit [25–27]. Thus, a next essential ingredient for considering in this model is generalized boundary conditions. This approach was presented in Refs. [21], [36], and [37], where the boundary condition was assumed to be

$$\mathcal{J}_{\pm}\left(\pm d/2, t\right) = \pm\int_0^1 d\bar{\nu}\int_{-\infty}^{t} dt'\kappa(t-t',\bar{\nu})\partial_{t'}^{\bar{\nu}} n_{\pm}\left(\pm d/2, t'\right) , \tag{19}$$

where the choice of $\kappa(t,\bar{\nu})$ is related to the surface effect presented by the surface such as adsorption–desorption [21] and charge transfer [33]. This general condition recovers several situations and leads to a scenario characterized by anomalous diffusion, as discussed in Refs. [38] and [39].

The impedance obtained when considering the condition (19) is given by [21,36,37]

$$\mathcal{Z}_{\text{PNPA}} = \frac{\bar{\mathcal{Z}}}{i\psi\beta^2}\frac{\Upsilon/\beta + \mathcal{M}E(i\omega)}{1 + \left[\beta\left(1+i\psi\right)\Upsilon/(i\psi\omega_{\mathcal{D}}\lambda_{\mathcal{D}})\right]\bar{\kappa}(i\omega)}, \tag{20}$$

where $\Upsilon = \tanh(\beta\mathcal{M})$, $E(i\omega) = i\psi + [\beta\Upsilon/(\lambda_{\mathcal{D}}\omega_{\mathcal{D}})]\bar{\kappa}(i\omega)$, and $\bar{\kappa}(i\omega) = e^{-i\omega t}\int_0^1 d\nu(i\omega)^{\nu}\int_{-\infty}^{t}\kappa_{\alpha}(t-t',\nu)e^{i\omega t'}dt'$. By employing the same approximations used for the previous case, we can show

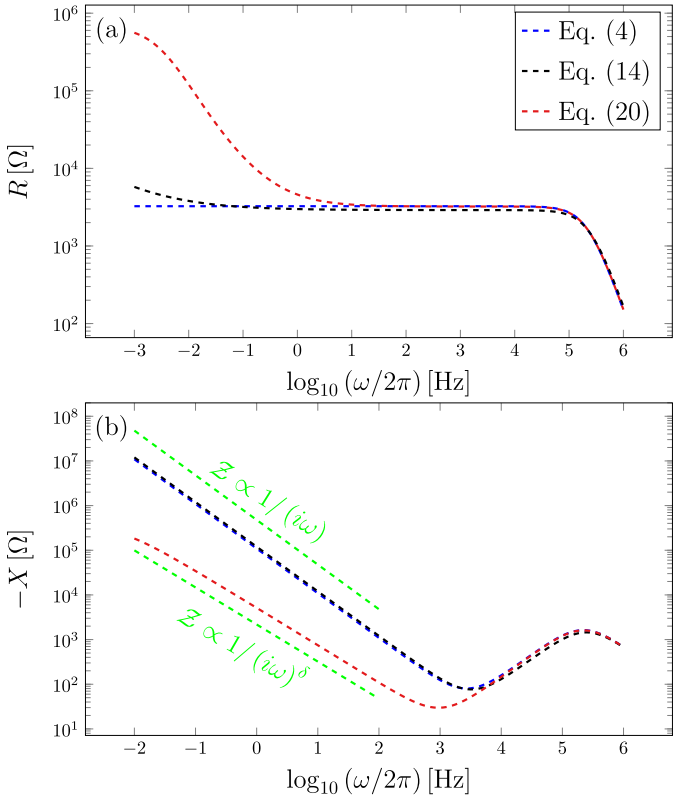

Fig. 3. Behavior of the real and imaginary parts of Eqs. (4), (14), and (20). For Eq. (20), we considered the condition $\bar{\kappa}(i\omega) = \bar{\kappa}_1 + \bar{\kappa}_2(i\omega)^{\delta_2}$. We also used $\mathcal{D} = 8\times10^{-9}\text{m}^2\text{s}^{-1}$, $\lambda_{\mathcal{D}} = 7.61\times10^{-8}$m, $\epsilon = 80\epsilon_0$, $q = 1.6\times10^{-19}$C, $S = 3.14\times10^{-4}\text{m}^2$, $d = 10^{-3}$m, $\mathcal{A} = 0.9$, $\gamma = 0.6$, $\delta_2 = 0.83$, $\bar{\kappa}_1 = 9.5\times10^{-8}\text{ms}^{-1}$, and $\bar{\kappa}_2 = 1.47\times10^{-5}\text{ms}^{-1}$. Similar to Fig. 1, we used green dotted lines as a guide for the behavior exhibited for the imaginary part of the impedance.

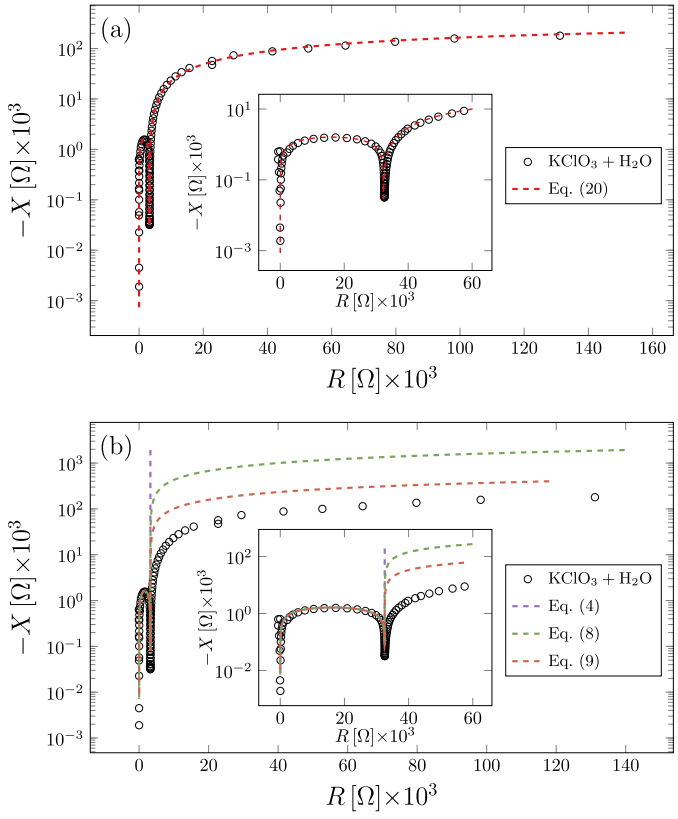

Fig. 4. The Nyquist diagram for the experimental data of $KClO_3$ (black dotted line) and the models. This figure also shows the behavior of Eqs. (4), (8), (9), and (20). Note that the best agreement between the experimental data and the theoretical model is obtained for the case Eq. (20). We used $\mathcal{D} \approx 8.0\times10^{-9}\text{m}^2\text{s}^{-1}$, $\lambda_{\mathcal{D}} \approx 7.61\times10^{-8}$m, $\epsilon \approx 80.0\epsilon_0$, $q = 1.6\times10^{-19}$C, $S = 3.14\times10^{-4}\text{m}^2$, $d = 10^{-3}$m, $\kappa_{\mathcal{G}} = 5\times10^{-8}\text{ms}^{-1}$, $\kappa_0 = 2\times10^9(\text{V m s})^{-1}$, $\bar{\kappa}_1 = 9.5\times10^{-8}\text{ms}^{-1}$, $\delta_2 = 0.83$, and $\bar{\kappa}_2 = 1.47\times10^{-5}\text{ms}^{-1}$.

that the asymptotic behavior in the low frequency limit for the impedance of the Eq. (20) is

$$\mathcal{Z}_{\rm PNPA} \approx \frac{2\lambda_{\mathcal{D}}}{\varepsilon S}\frac{1}{i\omega + \bar{\kappa}(i\omega)/\lambda_{\mathcal{D}}} + \frac{\lambda_{\mathcal{D}}^2 d}{\varepsilon S D} \quad . \tag{21}$$

The real part of Eq. (21) is directly related to bulk effects. The imaginary part exhibits a dependence on $\bar{\kappa}(i\omega)$, and consequently, shows how the surface affects the system in the low frequency limit. By a suitable choice of $\bar{\kappa}(i\omega)$, the impedance predicted by this model is able to reproduce the experimental data of Fig. 2. In fact, for $\bar{\kappa}(i\omega) \propto (i\omega)^{\delta}$ with $0 < \delta \leq 1$, the asymptotic behavior of the experimental data (see Fig. 2) is correctly reproduced by Eq. (21).

In order to completely describe the experimental data of Fig. 2, we consider $\bar{\kappa}(i\omega) = \bar{\kappa}_1 + \bar{\kappa}_2 (i\omega)^{\delta_2}$. This choice leads to charge transfer behavior followed by a capacitive behavior exhibited by $\delta_2 \neq 1$, which may be associated to an accumulation and/or adsorption–desorption process on the electrode surfaces. Furthermore, this choice for $\bar{\kappa}(i\omega)$ can be related (in the low frequency limit) to the admittance/impedance obtained in Ref. [25] for the Helmholtz layer. In the case of blocking electrodes discussed in Ref. [25], we have to consider $\bar{\kappa}_1 = 0$ and relate $\bar{\kappa}_2$ with the resistance of the compact (Helmholtz) layer and its relaxation time; thus, the capacitance dispersion is characterized by δ_2. For the case of partially blocking electrode, we have to consider $\bar{\kappa}_1 \neq 0$ and relate it with the charge transfer resistance. Figure 4(a) shows a comparison between this model [Eq. (20)] and the experimental data obtained for a solution of $KClO_3$, where excellent agreement is observed. The comparison with the other models is shown in Fig. 4(b). In contrast with the results obtained for the model of the Eq. (20), we observe that the models of the Eqs. (4), (8), and (9) are not able to describe the experimental data for all frequency ranges.

4. Discussion and Conclusions

We have analyzed the asymptotic behavior in the low frequency limit of several impedance models. Starting by the standard PNP model with perfect blocking electrodes, we showed that this case only admits charge accumulation on the electrode surface. We also showed that, in the limit $\omega \to 0$, the real part of the impedance is characterized by a plateau and the imaginary part displays a purely capacitive behavior. When comparing with an experimental data, we verified that this model cannot describe the empirical behavior in all frequency ranges.

Next, we considered the Chang-Jaffe and the Ohmic boundary conditions, which are usually associated to charge transfers from the electrolyte and the external circuit by means of electrochemical reactions. In both cases, the low frequency limit of the impedance is characterized by an inductive behavior for the imaginary part, and by a plateau for real part of the impedance. These results show the effects of boundary conditions on the formal results obtained for the impedance in each case. In particular, these asymptotic limits of imaginary part of the impedance are in contrast with the standard PNP model with perfect blocking electrodes, in which purely capacitive behavior was observed.

However, we discussed that simple experimental data (as the ones shown in Fig. 2) display empirical behaviors (especially, in the low frequency limit) that cannot be described by the three previous-mentioned models. Because of that, we considered models based on the presence of fractional time derivatives in the bulk equation and in the boundary conditions. We further verified that alone, fractional time derivatives in the bulk equation are not enough for describing the experimental data in all frequency range. On the other hand, an excellent agreement with the experimental data is obtained when considering fractional time derivatives on the boundary conditions. In particular, such boundary conditions are suitable for modeling the interplay between different effects, which can also be connected to different diffusive regimes. Finally, we hope that the results presented here may be useful to investigate the electrical response of several experimental systems as well as assist researchers to find the best framework for modeling their data.

Acknowledgments

We thank CNPq for the partial financial support.

Appendix A. APPROXIMATIONS FOR $\omega \to 0$

The asymptotic limit in the low frequency regime, where $\psi \to 0$ (*i.e.*, $\omega \to 0$), of Eq. (4) may be obtained by using the following approximation: $1/\beta \sim 1 - i\psi/2$. We also consider $d/\lambda_{\mathcal{D}} \gg 1$, implying that $\tanh(\mathcal{M}\beta) \sim 1$ (see Ref. [30] for more details). Under these assumptions, Eq. (4) can be written as follows

$$\mathcal{Z} \approx \left(\tilde{\mathcal{Z}}/\left(i\psi\right)\right)\left(1 + \mathcal{M}i\psi + \mathcal{O}(\psi^2)\right) \tag{22}$$

Thus, the main contributions for the real ($R_B = Re(\mathcal{Z})$) and imaginary ($X_B = Im(\mathcal{Z})$) parts of the impedance given by Eqs. (6) and (7) can be obtained from the previous equation. Equations (8) and (9), in this asymptotic limit, under the previous conditions yield

$$\begin{aligned} \mathcal{Z}_{CJ} &\approx \tilde{\mathcal{Z}}\left(\mathcal{M} + 1/\mathcal{H}\right) \\ &- \left(\tilde{\mathcal{Z}}/\mathcal{H}^2\right)\left(1 + 2\mathcal{H} + \mathcal{H}^2\mathcal{M}\right) i\psi + \mathcal{O}(\psi^2) \end{aligned} \tag{23}$$

and

$$\begin{aligned} \mathcal{Z}_{O} &\approx \tilde{\mathcal{Z}}\left(1 - 1/\mathcal{M} + 1/\left(\mathcal{M}\psi_q\right)\right) \\ &- \left(\tilde{\mathcal{Z}}/(2\mathcal{M}\psi_q)\right)\left(2 + \psi_q + 2\mathcal{M}\psi_q^2\right) i\psi + \mathcal{O}(\psi^2) \quad . \end{aligned} \tag{24}$$

From these equations, Eqs. (10), (11), (12), and (13) can be obtained after using the definition of the constants $\tilde{\mathcal{Z}}$, $\mathcal{H}$, $\mathcal{M}$, and ψ_q. The asymptotic limit of Eq. (14), given by Eqs. (17) and (18), can be obtained by using the approximation $1/\tilde{\beta} \sim 1 - \left(\mathcal{A}i\psi + \mathcal{B}\omega_{\mathcal{D}}^{\gamma-1}(i\psi)^{\gamma}\right)/2$ for $\gamma > 1/2$, under the condition $d/\lambda_{\mathcal{D}} \gg 1$ which implies in $\tanh(\mathcal{M}\tilde{\beta}) \sim 1$, it is possible to show that

$$\mathcal{Z}_F \approx \left(\tilde{\mathcal{Z}}/\left(i\psi\right)\right)\left(1 + \mathcal{M}\left(\mathcal{A}i\psi + \mathcal{B}\omega_{\mathcal{D}}^{\gamma-1}(i\psi)^{\gamma}\right) + \mathcal{O}(\psi^{2\gamma})\right). \tag{25}$$

Similar to the cases worked above, it is possible to obtain Eq. (21) from Eq. (20) by considering the limit of low frequency limit with $\kappa(i\omega) \sim 1/(i\omega)^{\delta}$ in the limit $\omega \to 0$.

References

[1] C.H. Chen, J. Liu, K. Amine, Symmetric cell approach and impedance spectroscopy of high power lithium-ion batteries, Journal of Power Sources 96 (2) (2001) 321–328, http://dx.doi.org/10.1016/S0378-7753(00)00666-2.
[2] R.G. Jungst, G. Nagasubraamanian, H.L. Case, B.Y. Liaw, A. Urbina, T.L. Paez, D.H. Doughty, Accelerated calendar and pulse life analysis of lithium-ion cells, Journal of Power Sources 119-121 (2003) 870–873, http://dx.doi.org/10.1016/S0378-7753(03)00193-9.
[3] M. Itagaki, N. Kobari, S. Yotsuda, K. Watanabe, S. Kinoshita, M. Ueb, $LiCoO_2$ electrode/electrolyte interface of Li-ion rechargeable batteries investigated by in situ electrochemical impedance spectroscopy, Journal of Power Sources 148 (2005) 78–84, http://dx.doi.org/10.1016/j.jpowsour.2005.02.007.
[4] D. Andre, M. Meiler, K. Steiner, Ch. Wimmer, D.U. Sauer, Characterization of high-power lithium-ion batteries by electrochemical impedance spectroscopy. I. Experimental investigation, Journal of Power Sources 196 (12) (2011) 5334–5341, http://dx.doi.org/10.1016/j.jpowsour.2010.12.102.
[5] M.A. Danzer, E.P. Hofer, Electrochemical parameter identification - An efficient method for fuel cell impedance characterisation, Journal of Power Sources 183 (1) (2008) 55–61, http://dx.doi.org/10.1016/j.jpowsour.2008.04.071.
[6] M.A. Danzer, E.P. Hofer, Analysis of the electrochemical behaviour of polymer electrolyte fuel cells using simple impedance models, Journal of Power Sources 190 (1) (2009) 25–33, http://dx.doi.org/10.1016/j.jpowsour.2008.10.003.

[7] M. Mamlouk, K. Scott, Analysis of high temperature polymer electrolyte membrane fuel cell electrodes using electrochemical impedance spectroscopy, Electrochimica Acta 56 (16) (2011) 5493–5512, http://dx.doi.org/10.1016/j.electacta.2011.03.056.
[8] D. Aaron, A.P. Borole, S. Yiacoumi, C. Tsouris, Effects of operating conditions on internal resistances in enzyme fuel cells studied via electrochemical impedance spectroscopy, Journal of Power Sources 201 (2012) 59–65, http://dx.doi.org/10.1016/j.jpowsour.2011.10.105.
[9] S.M.R. Niya, M. Hoorfar, Study of proton exchange membrane fuel cells using electrochemical impedance spectroscopy technique - A review, Journal of Power Sources 240 (2013) 281–293, http://dx.doi.org/10.1016/j.jpowsour.2013.04.011.
[10] V.F. Lvovich, M.F. Smiechowski, Electrochemical impedance spectroscopy analysis of industrial lubricants, Electrochimica Acta 51 (8-9) (2006) 1487–1496, http://dx.doi.org/10.1016/j.electacta.2005.02.135.
[11] V.F. Lvovich, M.F. Smiechowski, Non-linear impedance analysis of industrial lubricants, Electrochimica Acta 53 (25) (2008) 7375–7385, http://dx.doi.org/10.1016/j.electacta.2007.12.014.
[12] C. Grosse, A. Delgado, Dielectric dispersion in aqueous colloidal systems, Current Opinion in Colloid & Interface Science 15 (3) (2010) 145–159, http://dx.doi.org/10.1016/j.cocis.2009.11.004.
[13] A.D. Hollingsworth, Remarks on the determination of low-frequency measurements of the dielectric response of colloidal suspensions, Current Opinion in Colloid & Interface Science 18 (2) (2013) 157–159, http://dx.doi.org/10.1016/j.cocis.2013.01.002.
[14] P. Knauth, Ionic conductor composites: Theory and materials, Journal of Electroceramics 18 (2) (2000) 111–125, http://dx.doi.org/10.1023/A:1009906101421.
[15] P. Knauth, H.L. Tuller, Solid-state ionics: Roots, status, and future prospects, Journal of the American Ceramic Society 85 (7) (2002) 1654, http://dx.doi.org/10.1111/j.1151-2916.2002.tb00334.x.
[16] C. Krishnan, M. Garnett, New insights into the double layer structure from impedance measurements: Implications for biological systems, Electrochimica Acta 51 (8-9) (2006) 1541–1549, http://dx.doi.org/10.1016/j.electacta.2005.02.133.
[17] M. Naumowicz, A.D. Petelska, Z.A. Figaszewski, Impedance analysis of a phosphatidylcholine-phosphatidylethanolamine system in bilayer lipid membranes, Electrochimica Acta 51 (24) (2006) 5024–5028, http://dx.doi.org/10.1016/j.electacta.2006.03.038.
[18] H. Jun, L.T.M. Dao, S. Cho, Electrical impedance detection of senescence in adipose tissue-derived stem cells, Procedia Engineering 47 (2012) 1025–1028, http://dx.doi.org/10.1016/j.proeng.2012.09.323.
[19] H. Jun, L.T.M. Dao, S.C.J. Pyun, Effect of cell senescence on the impedance measurement of adipose tissue-derived stem cells, Enzyme and Microbial Technology 53 (5) (2013) 302–306, http://dx.doi.org/10.1016/j.enzmictec.2013.07.001.
[20] R. Metzler, J. Klafter, The random walk's guide to anomalous diffusion: a fractional dynamics approach, Physics Reports 339 (1) (2000) 1–77, http://dx.doi.org/10.1016/S0370-1573(00)00070-3.
[21] E.K. Lenzi, M.K. Lenzi, F.R.G.B. Silva, G. Gonçalves, R. Rossato, R.S. Zola, L.R. Evangelista, A framework to investigate the immittance responses for finite length-situations: Fractional diffusion equation, reaction term, and boundary conditions, Journal of Electroanalytical Chemistry 721 (2014) 82–88, http://dx.doi.org/10.1016/j.jelechem.2013.10.026.
[22] T. Pajkossy, L. Nyikos, Scaling-law analysis to describe the impedance behavior of fractal electrodes, Physics Review B 42 (1990) 709–719, http://dx.doi.org/10.1103/PhysRevB.42.709.
[23] H. Sanabria, J.H. Miller, Relaxation processes due to the electrode-electrolyte interface in ionic solutions, Physics Review E 74 (2006) 051505, http://dx.doi.org/10.1103/PhysRevE.74.051505.
[24] T. Kosztolowicz, K.D. Lewandowska, Hyperbolic subdiffusive impedance, Journal of Physics A: Mathematical and Theoretical 42 (2009) 055004, http://dx.doi.org/10.1088/1751-8113/42/5/055004.
[25] M.B. Singh, R. Kant, Debye-Falkenhagen dynamics of electric double layer in presence of electrode heterogeneities, Journal of Electroanalytical Chemistry 704 (2013) 197–207, http://dx.doi.org/10.1016/j.jelechem.2013.07.007.
[26] M.B. Singh, R. Kant, Theory of anomalous dynamics of electric double layer at heterogeneous and rough electrodes, Journal of Physical Chemistry C 118 (2014) 5122–5133, http://dx.doi.org/10.1021/jp410999b.
[27] M.B. Singh, R. Kant, Theory for anomalous electric double-layer dynamics in ionic liquids, Journal of Physical Chemistry C 118 (2014) 8766–8774, http://dx.doi.org/10.1021/jp500383p.
[28] J. Randles, Kinetics of rapid electrode reactions, Discussions of the Faraday Society 1 (1947) 11–19, http://dx.doi.org/10.1039/DF9470100011.
[29] B. Ershler, Investigation of electrode reactions by the method of charging-curves and with the aid of alternating currents, Discussions of the Faraday Society 1 (1947) 269–277, http://dx.doi.org/10.1039/DF9470100269.
[30] G. Barbero, L.R. Evangelista, Adsorption Phenomena and Anchoring Energy in Nematic Liquid Crystals, CRC Press, 2005.
[31] E.K. Lenzi, P.R.G. Fernandes, T. Petrucci, H. Mukai, H.V. Ribeiro, Anomalous-diffusion approach applied to the electrical response of water, Physical Review E 84 (2011) 041128, http://dx.doi.org/10.1103/PhysRevE.84.041128.
[32] E.K. Lenzi, P.R.G. Fernandes, T. Petrucci, H. Mukai, H.V. Ribeiro, M.K. Lenzi, G. Gonçalves, Anomalous diffusion and electrical response of ionic solutions, International Journal of Electrochemical Science 8 (2013) 2849–2862.
[33] H. Chang, G. Jaffe, Polarization in electrolytic solutions. part i. theory, The Journal of Chemical Physics 20 (1952) 1071–1077, http://dx.doi.org/10.1063/1.1700669.
[34] I. Lelidis, J.R. Macdonald, G. Barbero, Poisson-Nernst-Planck model with chang-jaffe, diffusion, and ohmic boundary conditions, Journal of Physics D: Applied Physics 49 (2016) 025503, http://dx.doi.org/10.1088/0022-3727/49/2/025503.
[35] E.K. Lenzi, L.R. Evangelista, G. Barbero, Fractional diffusion equation and impedance spectroscopy of electrolytic cells, Journal Physical Chemstry B 113 (2009) 11371–11374, http://dx.doi.org/10.1021/jp904741m.
[36] E.K. Lenzi, J.L. de Paula, F.R.G.B. Silva, L.R. Evangelista, A connection between anomalous Poisson-Nernst-Planck model and equivalent circuits with constant phase elements, Journal of Chemical Physics C 117 (2013) 23685–23690, http://dx.doi.org/10.1021/jp4063725.
[37] F.R.G.B. Silva, H.V. Ribeiro, M.K. Lenzi, T. Petrucci, F.S. Michels, E.K. Lenzi, Fractional diffusion equations and equivalent circuits applied to ionic solutions, International Journal of Electrochemical Science 9 (2014) 1892–1901.
[38] E.K. Lenzi, L. Evangelista, G. Barbero, F. Mantegazza, Anomalous diffusion and the adsorption-desorption process in anisotropic media, EPL (Europhysics Letters) 85 (2009) 28004, http://dx.doi.org/10.1209/0295-5075/85/28004.
[39] E.K. Lenzi, C.A.R. Yednak, L.R. Evangelista, Non-Markovian diffusion and the adsorption-desorption process, Physical Review E 81 (2010) 011116, http://dx.doi.org/10.1103/PhysRevE.81.011116.